

http://pubs.acs.org/journal/aelccp

# Nanoscale Elemental Mapping of Intact Solid— Liquid Interfaces and Reactive Materials in Energy Devices Enabled by Cryo-FIB/SEM

Michael J. Zachman, Zhengyuan Tu, Lynden A. Archer, and Lena F. Kourkoutis\*



Cite This: ACS Energy Lett. 2020, 5, 1224–1232



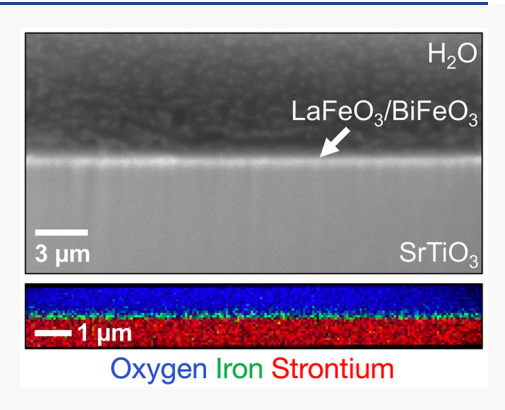
**ACCESS** 

Metrics & More



Supporting Information

ABSTRACT: Many modern energy devices rely on solid—liquid interfaces, highly reactive materials, or both, for their operation and performance. The difficulty of characterizing such materials means these devices often lack high-resolution characterization in an unaltered state. Here, we demonstrate how cryogenic sample preparation and transfer can extend the capabilities of FIB/SEM techniques to solid—liquid interfaces and reactive materials common to energy devices by preserving their integrity through all stages of preparation and characterization. We additionally show how cryo-FIB/SEM paired with energy dispersive X-ray spectroscopy enables nanoscale elemental mapping of cross-sections produced in these materials and discuss strategies to achieve optimal results. Finally, we consider current limitations of the technique and propose future developments that could enhance its capabilities. Our results illustrate that cryo-FIB/SEM will be a useful technique for fields where solid—liquid interfaces are results in the formation of the results and these formations are the solid—liquid interfaces are results.



interfaces or reactive materials play an important role and could, thus far, not be characterized at high resolution.

evices that rely on solid-liquid interfaces or reactive materials are ubiquitous in modern society and will continue to play an important role in the future. Examples are dye-sensitized solar cells for energy generation, fuel cells for electrolysis and conversion of fuels to electricity,<sup>2</sup> and supercapacitors and batteries for energy storage.<sup>3,4</sup> Energy devices such as these, however, present a problem for characterization since they contain liquids and/or highly reactive materials. Typically, liquids are removed before characterization in high-vacuum instruments to prevent immediate evaporation. The associated washing and drying process can, however, result in structural and chemical modifications of soft or brittle materials present at the sample interface.<sup>5</sup> Samples containing highly reactive materials, such as alkali metals, present additional challenges for characterization since exposed regions react quickly with air during transfer to the instrument or with contaminants in the vacuum during characterization, altering the sample's surface chemistry.

While the devices mentioned above are macroscopic in size, the electrode structures and processes at the solid—liquid interfaces inside may have features down to the nanoscale. A technique capable of bridging this significant size gap is therefore needed to study these features within actual devices. Focused ion beam/scanning electron microscopy (FIB/SEM) techniques combine the milling capability of a FIB with the imaging and spectroscopic capabilities of an SEM to enable

nanoscale characterization of surface and cross-sectional structures on samples up to tens of centimeters in size. These techniques are used commonly in both academia and industry for characterization, failure analysis, and editing of solid devices such as silicon wafers and integrated circuits, microelectrical-mechanical systems, and solid-state batteries. Despite the power and versatility of FIB/SEM techniques, they have traditionally been limited to solid samples due to the issues discussed above and nonreactive materials due to interactions with the commonly used gallium ion beam.

Recently, cryogenic-electron microscopy techniques used for imaging small biological molecules and cells<sup>12</sup> have been adapted for cryo-FIB preparation of intact solid—liquid interfaces for high-resolution cryo-scanning transmission electron microscopy (STEM) characterization.<sup>13,14</sup> While STEM techniques can provide structural, elemental, and bonding information down to the atomic scale, typical sample dimensions are on the order of microns across and under 100

Received: January 28, 2020 Accepted: March 16, 2020 Published: March 16, 2020



nm thick, while many functional devices have dimensions on the order of centimeters. A technique that allows more rapid characterization of larger sample volumes while maintaining reasonably high resolution would therefore be valuable for providing a broader view of the structure and elemental composition of features in devices.

Pairing FIB/SEM with cryogenic techniques would allow this broader view of energy materials and devices to be obtained while still preserving reactive materials and solidliquid interfaces. Cryogenic sample temperatures in the FIB have previously been utilized to improve milling characteristics for a variety of materials, such as III-V semiconductor devices, 15 minerals, 16 thin film solar cells, 17 and human dentin/ enamel, <sup>18,19</sup> and initial demonstrations of cryo-FIB techniques that enable imaging of larger volumes of deposited lithium have recently been shown. <sup>14,20,21</sup> In addition, cryo-FIB has become a valuable tool in biology, where it enables frozenhydrated specimens to be either directly milled and characterized<sup>22,23</sup> in the FIB/SEM or prepared for cryo-TEM.<sup>24–31</sup> Here, we illustrate the benefits of cryogenic sample preparation and transfer for characterization of devices containing solid-liquid interfaces and reactive materials in the FIB/SEM and extend the capabilities of cryo-FIB/SEM to nanoscale spectroscopic mapping. We show that by rapid freezing and careful cryogenic sample transfer into the instrument, liquids and soft materials present at interfaces are preserved, and exposed reactive materials experience minimal changes in surface composition during transfer. The cryogenic sample temperature is thought to slow down the chemical kinetics of reactive materials sufficiently to enable milling, without significant interactions with contaminants in the vacuum or alloying with the gallium ions, as is the case at room temperature. We demonstrate these techniques using bare lithium metal electrodes, lithium deposited on an electrode with an artificial solid-electrolyte interphase (SEI) layer in a coin cell battery, and aqueous solution-solid oxide interfaces. By performing imaging and spectroscopic mapping on cross-sections produced by cryo-FIB milling, we reveal the morphology and elemental composition of the unaltered materials and intact interfacial layers present and demonstrate that the structure and elemental composition of these features can be characterized down to the nanoscale. Methods for achieving optimal results are discussed, in addition to limitations of these techniques and future developments that could broaden the capabilities of cryo-FIB/SEM.

To prepare coin cell batteries for characterization by cryo-FIB, the cells are manually opened and the electrode of interest is removed for plunge-freezing. A schematic of a typical coin cell configuration is shown in Figure 1a. For many experiments, the reactive electrode surface is protected from interaction with air during the brief transfer into the slush nitrogen pot by the liquid electrolyte on its surface. In order to test the minimum rate of transfer needed to avoid contamination under any conditions, however, we prepared dry coin cells with bare lithium metal electrodes inside. Electrodes that were removed from the cells and immediately (on the order of seconds) plunge-frozen in slush nitrogen showed no signs of contamination by SEM imaging (Figure 1b), limiting possible effects of a rapid transfer on exposed lithium to the nanoscale, similar to passivation layers observed previously at room temperature by in situ TEM.<sup>32</sup> Intentionally exposing the electrodes to air for approximately 1 min prior to plunge-freezing resulted in oxide formation initiating at specific

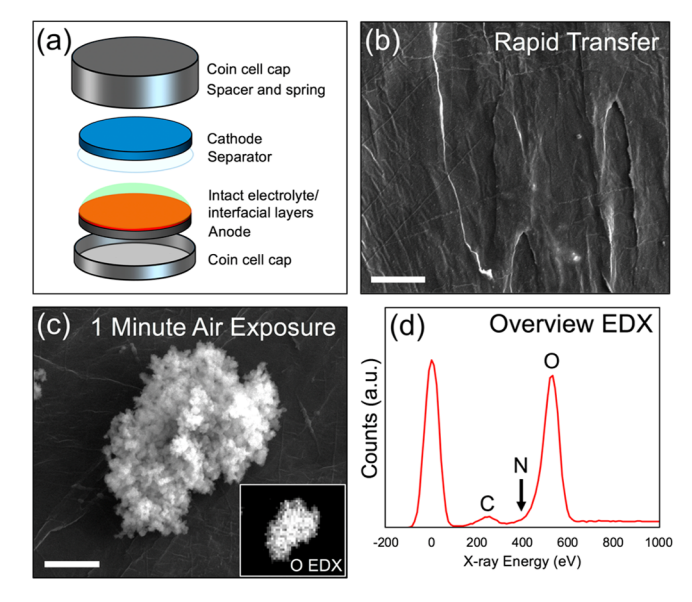


Figure 1. Stability of bare lithium metal during transfer of the electrode from a coin cell battery into the cryo-FIB. (a) A schematic of a typical coin cell used for cryo-FIB experiments, where the lower electrode, typically covered by an electrolyte, is removed and rapidly frozen in slush nitrogen. (b) SEM image of a rapidly transferred bare lithium electrode from a coin cell to the slush nitrogen pot shows no obvious surface reactions. (c) Intentional exposure to air for ~1 min before plunging into slush nitrogen results in formation of oxide growths at grain boundaries on the electrode surface as confirmed by EDX (inset). (d) EDX spectrum recorded on the lithium electrode from (b). Despite the direct contact with liquid/solid nitrogen, no reaction with the lithium to form lithium nitride occurs during preparation. Scale bars, 3  $\mu$ m.

locations on the surface, such as grain boundaries. An example of one of these oxide growths is shown in Figure 1c, with the corresponding oxygen EDX map. An EDX spectrum of the lithium surface is also shown in Figure 1d. Additionally, while molecular nitrogen is generally considered inert due to its strong triple bond, the highly reducing nature of lithium provides the potential for a reaction to form lithium nitride, a potential concern for plunge-freezing in liquid or slush nitrogen. We found, however, that the cryogenic temperature of the nitrogen and the rapidly reduced sample temperature prevent these reactions from occurring, and nitrogen is not observed on the sample surface, for example, as displayed in the spectrum in Figure 1d. Therefore, rapid plunge-freezing of electrodes into slush nitrogen not only preserves liquids and interfacial structures present but also enables transfer into the instrument with minimal contamination. This is consistent with recent results that have shown how cryogenic transmission electron microscopy (TEM) techniques enable atomic-resolution imaging and nanoscale mapping of bonding environments in reactive and beam-sensitive materials, such as lithium, in an unaltered state. 14,33,34

With the sample maintained near liquid nitrogen temperature in the instrument, its chemical reactivity is dramatically reduced. This enables FIB milling of samples that are typically problematic at room temperature due to interactions with the gallium ion beam. For example, lithium can form alloys with gallium, <sup>35,36</sup> and this results in the formation of extraneous material during milling at room temperature, rather than a simple sputtering of the target material. Regular cross-sections

milled in lithium at room temperature therefore generate a large amount of redeposited material that covers the final cross-section surface (Figure 2a). The same milling performed

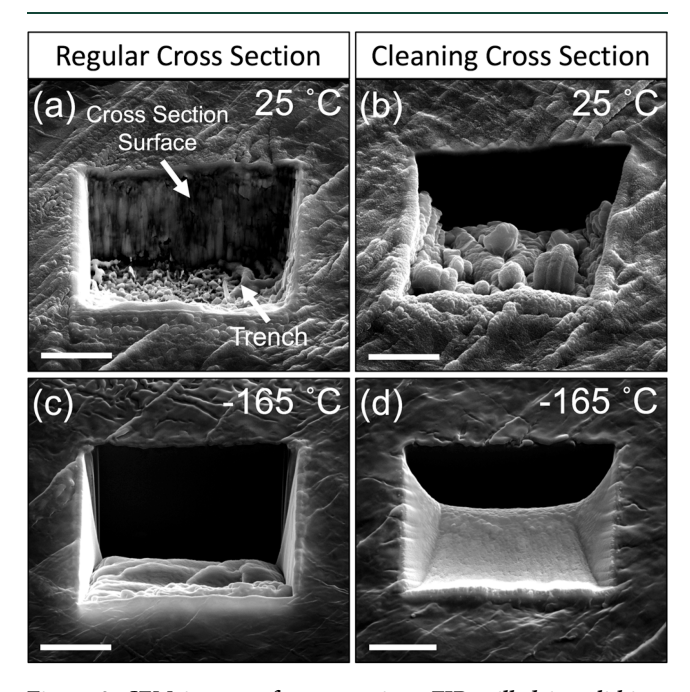


Figure 2. SEM images of cross-sections FIB milled into lithium metal held at room versus cryogenic temperature. (a) At room temperature a "regular cross-section", which removes material quickly by making multiple milling passes over the sample, results in the formation of extraneous material, likely a lithium—gallium alloy, which redeposits in the surrounding area and on the cross-section surface. (b) Likewise, a "cleaning cross-section", which makes a single slow milling pass over the sample to leave a clean cross-section surface, results in the formation of large structures in the trench, potentially blocking the view of the cross-section surface. Milling (c) regular cross-sections and (d) cleaning cross-sections with the sample cooled to cryogenic temperature, however, enables clean trenches and final cross-section surfaces to be produced in reactive materials such as lithium. Scale bars, 5  $\mu$ m.

with the sample at cryogenic temperature, however, produces a clean surface with very little redeposited material (Figure 2c). While cleaning cross-sections milled at room temperature do result in clean final cross-section surfaces, they generate large structures in the trench (Figure 2b) that are likely composed of a lithium-gallium alloy (see Figure S1) and can impede the view of the cross-section surface. Milling at cryogenic temperature significantly increases the quality of the milled area, and the material redeposited in the trench appears similar to that of materials that do not interact with the gallium beam at room temperature. It is also worth noting that the samples shown in Figure 2 were loaded into the FIB using the full cryogenic loading technique described above, and the sample was subsequently warmed to room temperature for the corresponding portion of the experiment. This enabled us to avoid the significant oxidation that the lithium surface undergoes during the extended loading period required for room temperature FIB preparation.

By preventing surface reactions and increasing the quality of the cross-sections through the use of cryogenic techniques, accurate characterization of reactive materials such as those used in batteries is enabled. An example of this is demonstrated in Figure 3. Here, lithium was deposited in coin cell batteries onto a copper electrode coated with a thin artificial SEI layer consisting of  $\sim$ 15 nm of alumina by atomic layer deposition (ALD). The cells were cycled three times in a 1 M LiTFSI in DOL/DME electrolyte with a current of 1 mA/cm² and a capacity of 0.5 mAh/cm².

Inhomogeneities in the alumina layer guided the deposition and resulted in formation of localized lithium deposits (Figure 3a). The cryogenic sample temperature allowed us to mill cleanly through the deposits, revealing their native interior structure, as shown in Figure 3b. Both dense and porous regions were found within the deposited lithium (marked by \*\* and \*, respectively), with differing contrast in the secondary electron images. In addition to imaging of cross-sections produced by cryo-FIB, EDX mapping can be performed to track the distribution of elements in the cross-section. This is shown in Figure 3c-f for the carbon, oxygen, aluminum, and copper signals present in the cross-section through the lithium deposit (see Figure S2 for gallium). First, the ~15 nm thick alumina layer can be seen in the aluminum map, indicating that layers at least this thin can be identified by EDX in the cryo-FIB. This layer is thin enough that the oxygen signal is likely much weaker than the signal coming from the lithium deposit, and therefore not visible adjacent to it. Additionally, while no elements were detected in the dense deposition regions, a significant concentration of oxygen and carbon was observed in the porous regions. Since low-energy Li K-edge X-rays are undetectable by most EDX spectrometers, the apparent lack of elements in the dense regions indicates these are areas of pure lithium deposition. In contrast, the material in the porous regions is likely composed of lithium oxide and/or carbonate, due to the combined oxygen and carbon signals in these regions. This suggests that porous or dendritic type lithium deposits may involve additional chemistry. Here, the advantages of cryo-FIB/SEM over conventional FIB/SEM are clear, since sample transfer, milling, and even exposure to the electron beam at room temperature can each induce compositional changes in sample. Cryogenic cooling enables characterization of the inherent nature of these materials, not possible by room temperature FIB/SEM.

In addition to enabling accurate characterization of clean cross-sections produced in reactive materials, the rapid freezing process preserves liquids present on the sample. This allows cross-sections to be produced through intact solid-liquid interfaces, enabling nanoscale imaging and spectroscopy of structures and layers at these often complex interfaces in their near-native environment. Figure 4 demonstrates these capabilities, displaying a cross-section milled through a droplet of aqueous solution in contact with an oxide substrate, similar in structure to a liquid-gated field-effect transistor.<sup>37,38</sup> Here, the sample was specifically designed to demonstrate resolution limits of the cryo-FIB/SEM technique. Between the strontium titanate (STO) substrate and the aqueous solution is a ~50 nm thick interfacial layer consisting of alternating lanthanum ferrite (LFO) and bismuth ferrite (BFO) unit cells produced by molecular beam epitaxy.<sup>39</sup> To form the small aqueous droplets on the surface, an atomizer was used to deposit the liquid. For this sample, approximately 2  $\mu$ m of organometallic platinum was deposited on the sample surface prior to milling to protect the soft aqueous material and enable a smooth final cross-section surface. Imaging of the interface revealed that the LFO/BFO interfacial layer was easily resolved, as displayed in Figure 4b. After accounting for the effect of the oblique

**ACS Energy Letters** 

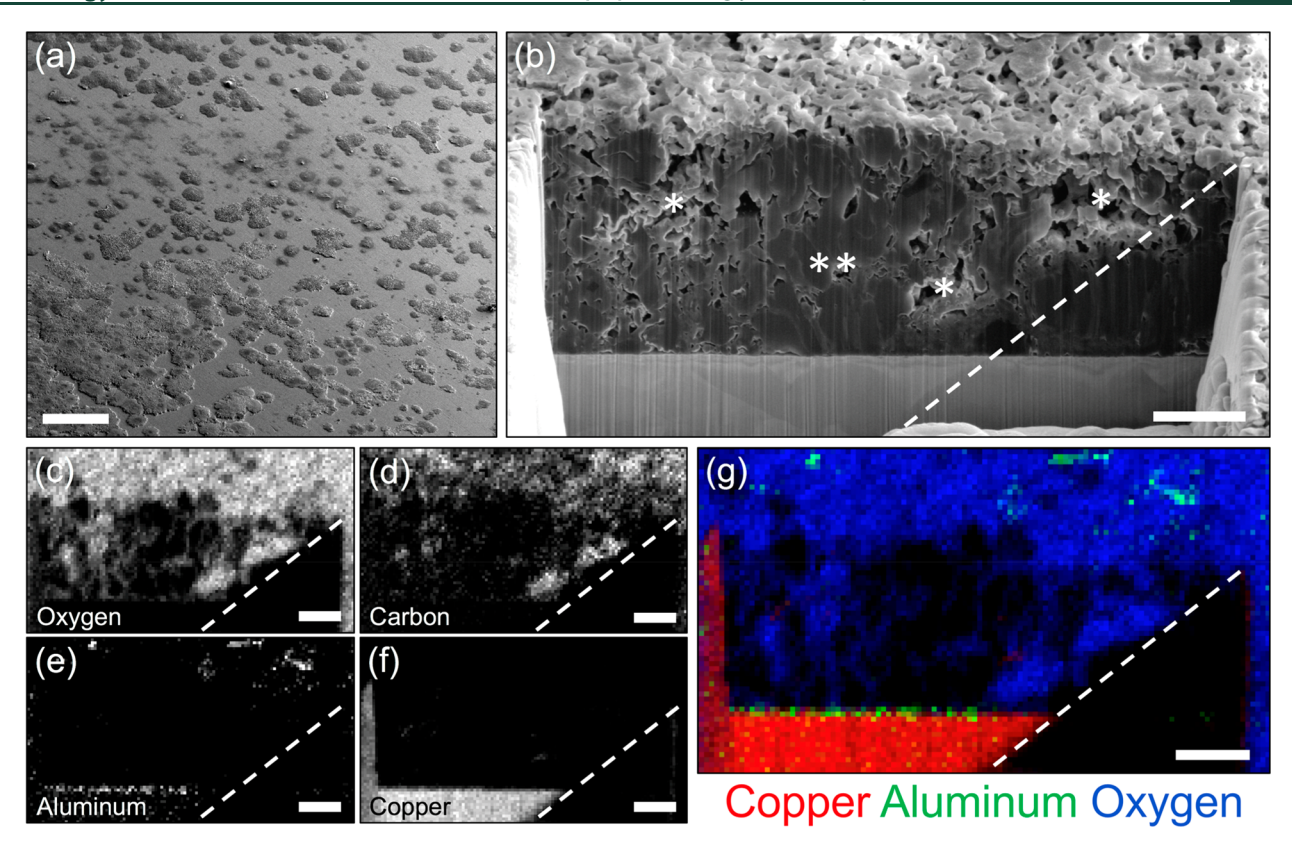


Figure 3. Nanoscale chemical mapping of interfaces in reactive materials. (a) Lithium was deposited on a copper current collector with a thin alumina artificial SEI layer  $\sim$ 15 nm thick, resulting in localized lithium deposits visible as patches on a uniform surface in the cryo-SEM image. (b) Cross-sectional cryo-FIB milling allowed internal dense and porous regions to be identified in the lithium deposits (marked by \*\* and \*, respectively). (c)–(g) Cryo-EDX mapping revealed no elements in the dense regions, indicating pure lithium deposition, but the porous regions contained elevated levels of carbon and oxygen, suggesting these regions contained lithium carbonates and oxides. These insights could not have been reliably provided by room temperature FIB/SEM due to sample reactions during transfer, milling, and characterization. Shadowing in the EDX maps, indicated by the dashed lines, is due to the placement of the detector. Scale bars, (a) 300  $\mu$ m and (b)–(g) 5  $\mu$ m.

imaging angle on the apparent thickness of the film, the resulting tilt-corrected full-width at half-maximum (fwhm) of the secondary electron signal from this layer was under 60 nm and therefore within 20% of the actual width of the layer. Additionally, spectroscopic mapping of the interface was performed, and the resulting oxygen, strontium, iron, bismuth, and lanthanum maps are shown in Figure 4c (see Figure S3 for gallium). While oxygen is present in all of the layers across the interface, the signal is strongest in the aqueous solution, and the strontium is present only in the substrate. The iron, bismuth, and lanthanum signals, however, are localized to the interfacial LFO/BFO layer, demonstrating that interfacial layers at least as thin as 50 nm can be mapped at intact solid-liquid interfaces by cryo-FIB EDX. A composite map of the oxygen, iron, and strontium signals is also shown in Figure 4d, along with a line profile of these elements across the interface. While the LFO/BFO layer is ~50 nm thick, the iron line profile displays a value larger than this, with a tilt-corrected fwhm of ~200 nm, which is discussed further in the Supporting Information. In addition, optimization of the spatial resolution of spectroscopic maps of solid-liquid interfaces by cryo-FIB/SEM requires many factors to be considered, such as sample geometry, beam accelerating voltage, and electron dose. As such, a detailed discussion on the optimization of spatial resolution in spectroscopic maps is also included in the Supporting Information.

While we have demonstrated the capabilities of cryo-FIB/ SEM by performing nanoscale imaging and spectroscopic mapping of cross-sections produced in a few example systems, these techniques will be beneficial for studying a wide range of phenomena in energy devices. Electrochemical energy storage, for example, often involves both chemically reactive materials and solid-liquid interfaces,4 and accurate characterization of these materials and interfaces is therefore difficult to achieve. The ability to directly image and map materials and interfaces in a near-native state will be very useful for studying processes at these interfaces. One area where this will be beneficial is in engineering of artificial SEI layers, which has been shown to be a promising method for improving the cyclability and safety of high-energy density rechargeable metal-anode batteries.<sup>40</sup> Cryogenic techniques allow the native thickness, morphology, and composition of artificial SEI layers to be tracked. Typically, engineering of these layers relies on ex situ experiments to monitor these characteristics, which could provide misleading results. As a result, cryo-FIB/SEM will enhance the design and implementation of artificial SEIs, advancing metal-anode battery technology. An additional area where cryo-FIB could prove useful for electrochemical energy storage is in tracking dissolution of elements from electrodes, an issue that limits various promising materials. For example, manganese oxide spinels are cathode materials that have generated interest due to their low cost, low environmental impact, high rate

ACS Energy Letters

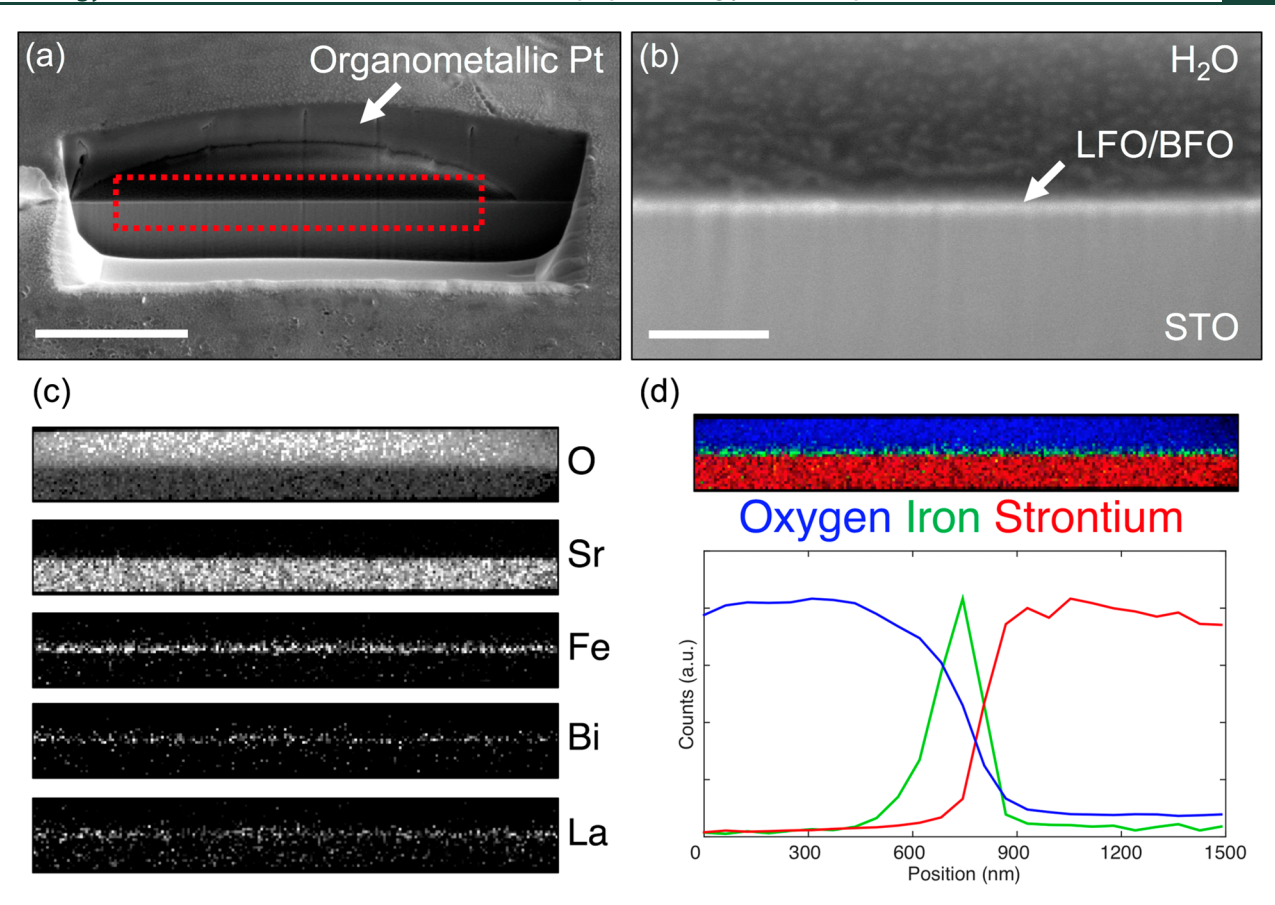


Figure 4. Nanoscale imaging and mapping of an intact solid—liquid interface cross-section. (a) A droplet of aqueous solution was rapidly frozen on the surface of a strontium titanate (STO) substrate, with a  $\sim$ 50 nm thick interfacial layer of alternating lanthanum ferrite/bismuth ferrite (LFO/BFO) unit cells. An organometallic platinum layer was deposited on the surface of the sample before milling to enable a smooth cross-section surface to be formed. (b) Cryo-SEM imaging of the interface confirmed the  $\sim$ 50 thick interfacial layer. (c) Cryo-EDX mapping of the interface revealed oxygen present throughout the sample but strongest in the aqueous solution, and strontium only in the substrate. A strong Fe-L signal and weaker La-M and Bi-M signals were present at the interface. (d) An integrated line profile of the iron signal showed a strong peak centered at the interface, with a tilt-corrected fwhm of around 200 nm due to beam penetration and broadening combined with the sample tilt. This is apparent on the aqueous solution side of the interface, where a tail in the iron signal is present. Scale bars, (a) 5  $\mu$ m and (b) 500 nm.

capability, and potential for operating at high voltages, but their longevity is limited by dissolution of Mn<sup>2+</sup> ions out of the cathode and into the electrolyte. 44-46 Cryo-FIB techniques may allow this dissolution process to be directly tracked with the electrolyte present, providing useful information to help circumvent this issue and enable use of these materials. Finally, cryogenic temperatures have also been shown to stabilize volatile solids in the instrument vacuum.<sup>47</sup> Therefore, cryo-FIB/SEM will enable accurate characterization of sulfurcontaining materials, for example, which is not possible using standard high-vacuum techniques at room-temperature. Sulfurbased cathodes are considered some of the most promising for viable lithium metal batteries but currently have performance that is limited by issues including dissolution of polysulfides into the electrolyte and shuttling of these materials between the electrodes. 48 Cryo-FIB techniques could therefore significantly aid the development of lithium-sulfur batteries by enabling accurate characterization of sulfur-based cathode structures designed to address these issues, and aid in evaluation of the effectiveness of these structures by tracking the corresponding polysulfide dissolution and shuttling in the

While cryo-FIB/SEM allows a wide variety of experiments to be performed that were not possible before, additional developments will continue to expand its capabilities in the future. Recently, for example, Xe+ plasma FIBs (PFIBs), which allow significantly larger quantities of material to be removed in a given time than traditional gallium-based FIBs, have been combined with SEM beams to form PFIB/SEM systems.49 Development of cryo-PFIB/SEM would broaden the capabilities of cryo-FIB techniques. For example, the increased milling rate could enable material to be removed from the edge of the sample all the way to the site of interest, providing a means to characterize interfaces away from the edge of the sample parallel to the electron beam. Cryo-PFIBs would also allow larger devices, or structures further buried within devices, to be characterized. For example, a cryo-PFIB may be able to mill entirely though small batteries. This would allow structures and elements to be tracked across the entire distance between the electrodes, rather than just the region near a single electrode.

An additional benefit of the cryogenic sample temperature could be enabling EDX of lithium over extended time periods. Due to its low energy, the lithium K-edge is typically not detectable by EDX. Recently though, EDX detectors capable of measuring the K-edge of lithium in high concentrations, such as in lithium metal, have been developed by decreasing the electronic noise and improving the charge collection efficiency

of the detectors, as well as removing the vacuum window between the detector and FIB/SEM chamber, which absorbs low-energy X-rays. <sup>50</sup> Similar to oxidation of lithium in the TEM, <sup>6</sup> exposing lithium metal to the electron beam in the SEM at room temperature will oxidize the surface of the sample, reducing the lithium signal over time. As a consequence, the lithium signal decreases over time for extended acquisitions, such as during elemental mapping. Pairing these new detectors with cryo-FIB/SEM, however, would minimize this effect and allow lithium to be mapped with increased signal over an extended period of time.

Finally, combining these cryo-FIB/SEM techniques with a cryogenic sample lift-out system enables preparation of cryo-STEM samples as well. This provides a pathway to combining the morphological and elemental information provided by cryo-FIB/SEM with higher resolution structural and bonding information provided by aberration corrected cryo-STEM techniques. This could allow, for example, dissolution of cathode materials to be tracked at very high resolution near the electrode surface. While the cryo-FIB/SEM approach is more limited in spatial resolution, it is comparatively simple and allows for rapid assessment of the structure and chemistry of interface layers, and their variation across large samples such as battery electrodes.

In each of these cases, development of improved equipment and techniques for preparation of devices such as batteries could help to reduce or eliminate environmental exposure of samples prior to entering the cryo-FIB/SEM. While the liquids in solid-liquid interfaces often protect the reactive materials in these devices and transfers are currently performed in seconds, this may not be sufficient for certain samples. As a result, future improvements to instrumentation and methods could reduce this time or eliminate exposure of samples to the environment prior to cryo-FIB/SEM altogether. For example, cells designed to be integrated with plunge-freezing hardware and automatically opened immediately prior to freezing could decrease the exposure time required. In addition, performing this step in an inert environment, such as in a glovebox, would minimize the concentration of reactive gases that the sample is exposed to. Developments such as these would help to ensure that accurate results are obtained.

While many devices important for current and future energy generation and storage rely on reactive materials and solidliquid interfaces, characterization of these types of materials at high resolution is often not possible. Cryo-FIB/SEM techniques combine the nanoscale imaging and spectroscopic capabilities of SEM and the milling capability of FIB with cryogenic sample temperatures, enabling unaltered reactive materials and intact solid-liquid interfaces from devices to be characterized at the nanoscale. These techniques will benefit a wide range of fields, allowing, for example, enhanced design and implementation of artificial SEI layers, tracking of material dissolution from electrodes, and accurate characterization of volatile solids such as sulfur. Cryo-FIB will therefore be an important tool for engineering devices that utilize reactive materials and/or solid-liquid interfaces, and further developments will continue to enhance its capabilities in the future.

## **■** EXPERIMENTAL METHODS

To enable the use of cryogenic sample temperatures in our FIB, the instrument was outfitted with a Quorum Technologies, Inc. PP3010T Cryo-FIB/SEM preparation system. This system includes a cold stage and anticontaminator in the

FIB, as well as a preparation chamber with a separate cold stage and anticontaminator, a workstation and liquid nitrogen pot, and a vacuum transfer device. Frozen samples are transferred from the workstation to the preparation chamber via the vacuum transfer device. Once in the preparation chamber, techniques such as metal sputter coating can be performed. The samples are then shuttled into the FIB chamber through a valve connecting the preparation chamber to the FIB. The cold stages in both the preparation and FIB chambers maintain the sample near liquid nitrogen temperature, typically -165 °C, while the anticontaminators are set at -192 °C to preferentially adsorb contaminants in the vacuum. These temperatures are measured by a thermocouple within each component and are accurate to within a few degrees Celsius near liquid nitrogen temperature. Temperatures can be set with a precision of 1 °C, and readings do not fluctuate once stabilized. The stability of the stage indicates that the sample temperature does not fluctuate noticeably during experiments.

To immobilize liquids present in samples, rapid freezing in a liquid or slush cryogen is used. Consideration of the type of liquid is necessary for choosing an appropriate cryogen. If the liquid must be vitrified, or preserved in an amorphous state, the cooling rate has to be larger than a critical value 12,51,52 that depends on thermal and physical properties of the liquid being frozen. Aqueous solutions are typically frozen in liquefied organic gases, such as propane, ethane, or a mixture of the two, 53 since they generate higher cooling rates than liquid or slush nitrogen.<sup>51</sup> If the sample contains organic liquids, however, organic cryogens can dissolve this material during the freezing process. 54-58 As a result, an alternative cryogen that does not interact with organic liquids must be chosen for these samples. Here, we use slush nitrogen for this purpose, which is produced by vacuum pumping on liquid nitrogen until it solidifies, followed by a pressure increase to atmospheric pressure. This results in a slush containing both solid and liquid nitrogen, with an enhanced cooling rate compared to liquid nitrogen since the Leidenfrost effect is avoided. Although slush nitrogen has a cooling rate lower than organic cryogens, the rate necessary for vitrification of organic liquids is less than that of aqueous solutions. 55,58 As a result, we have found that organic electrolytes up to at least microns thick on the surface of large samples such as coin cell battery electrodes can be vitrified by plunge-freezing in slush nitrogen.

Once the sample is frozen in the workstation, it is placed on a shuttle and the vacuum transfer device is attached to the liquid nitrogen pot. The transfer device is then pumped to a moderate vacuum (approximately 3 orders of magnitude below atmospheric pressure), and the shuttle is retracted into the transfer device, sealed inside a small vacuum chamber, and transferred to the preparation chamber attached to the FIB. Here, the sample surface is typically coated with 5–10 nm of metal, either platinum or gold–palladium, to increase its conductivity. For the sputter coater in the Quorum PP3010T preparation chamber, a current of 10 mA and a deposition time of 10 s were used. Once this process is complete, the sample is transferred through a valve to the cold stage in the FIB chamber.

In the FIB, imaging or spectroscopic mapping by energy dispersive X-ray spectroscopy (EDX) can be immediately performed on the sample surface to locate regions of interest. In certain cases, even subsurface features can be localized, since the accelerating voltages used (5–30 kV) enable the beam to penetrate below the sample surface.<sup>13</sup> The sample surface is

then tilted perpendicular to the Ga+ ion beam and a crosssection is milled site-specifically at the point of interest. Crosssections are typically 10 or 20 µm deep and of similar width, though larger or smaller regions can be milled on the basis of the material properties and the patience of the user. Milling typically takes place in two steps. First, a "regular cross-section" is milled at high beam current, on the order of nanoamps, to quickly remove a large amount of material. This milling pattern results in multiple passes over the defined area, with an increased number near the cross-section surface, resulting in a trench with a depth gradient. While this removes material quickly, a layer of redeposited material can be left on the final cross-section surface. To remove this material, a "cleaning cross-section" is used, which makes a single slow pass over the defined milling area, ending with a final mill at the crosssection surface, which leaves it free of redeposited material. This final step can also be performed with a lower ion beam current to reduce probe tails, minimizing the "curtaining" effect that produces a rough final cross-section surface. Some materials, however, produce redeposited debris that cannot be effectively removed by such a final cleaning step. In this case, a single cleaning cross-section must be used to mill the entire trench, including the final surface, in one pass.

To further increase the quality of the final cross-section surface when milling frozen soft or liquid samples, deposition of a platinum material on the sample surface prior to milling can be used, as has been shown for a biological specimen. Site-specific deposition of platinum metal is used regularly to aid room temperature preparation of TEM samples by FIB,8 but cryogenic sample temperatures result in the organometallic platinum precursor gas adsorbing to the sample surface. This results in an extended and non-site-specific deposition of the material. The broadly deposited material still has beneficial qualities for milling, however, and a deposition of around 2-3 µm provides sufficient protection from probe tails to significantly reduce curtaining. Unlike platinum metal, this organometallic material is nonconductive and charges under the electron beam without additional processing. To address this, a "curing" process is performed, where the material is exposed to the ion beam. 59 This exposure releases the organic portion of the molecule near the surface while leaving the platinum behind, resulting in a conductive surface. Using these techniques, it is possible to create a clean and smooth final cross-section surface that allows accurate high-resolution imaging and spectroscopic mapping to be performed.

#### ASSOCIATED CONTENT

#### **Solution** Supporting Information

The Supporting Information is available free of charge at https://pubs.acs.org/doi/10.1021/acsenergylett.0c00202.

Discussion regarding optimization of spatial resolution in spectroscopic maps and supporting figures comparing alternate methods for achieving high-resolution spectroscopic mapping of solid—liquid interfaces by cryo-FIB/SEM (PDF)

### AUTHOR INFORMATION

#### **Corresponding Author**

Lena F. Kourkoutis — School of Applied and Engineering Physics and Kavli Institute for Nanoscale Science, Cornell University, Ithaca, New York 14853, United States; orcid.org/0000-0002-1303-1362; Email: lena.f.kourkoutis@cornell.edu

#### **Authors**

Michael J. Zachman — School of Applied and Engineering Physics, Cornell University, Ithaca, New York 14853, United States; orcid.org/0000-0003-1910-1357

**Zhengyuan Tu** − Department of Materials Science and Engineering, Cornell University, Ithaca, New York 14853, United States; ocid.org/0000-0002-7291-6144

Lynden A. Archer — Department of Materials Science and Engineering and Robert Frederick Smith School of Chemical and Biomolecular Engineering, Cornell University, Ithaca, New York 14853, United States; orcid.org/0000-0001-9032-2772

Complete contact information is available at: https://pubs.acs.org/10.1021/acsenergylett.0c00202

#### **Notes**

The authors declare no competing financial interest.

#### ACKNOWLEDGMENTS

We thank Colin Heikes, Julia A. Mundy, Zhe Wang, and Darrel G. Schlom for providing the oxide sample and John Grazul for his assistance with the method for preparing the aqueous solution droplets. M.J.Z. and L.F.K. acknowledge support by the NSF (DMR-1654596), the Center for Alkaline-Based Energy Solutions (CABES), part of the Energy Frontier Research Center (EFRC) program supported by the U.S. Department of Energy, under grant DE-SC-0019445, and the Packard Foundation. This work made use of the Cornell Center for Materials Research (CCMR) Shared Facilities with funding from the NSF MRSEC program (DMR-1719875). Additional support for the FIB/SEM cryo-stage and transfer system was provided by the Kavli Institute at Cornell and the Energy Materials Center at Cornell, DOE EFRC BES (DE-SC0001086). The work also made use of electrochemical characterization facilities in the KAUST-CU Center for Energy and Sustainability, supported by the King Abdullah University of Science and Technology (KAUST) through Award KUS-C1-018-02.

#### REFERENCES

- (1) Hagfeldt, A.; Boschloo, G.; Sun, L.; Kloo, L. Dye-Sensitized Solar Cells. Chem. Rev. 2010, 110, 6595–6663.
- (2) Stamenkovic, V. R.; Strmcnik, D.; Lopes, P. P.; Markovic, N. M. Energy and Fuels from Electrochemical Interfaces. *Nat. Mater.* **2017**, *16*, 57.
- (3) Zhang, L. L.; Zhao, X. S. Carbon-Based Materials as Supercapacitor Electrodes. *Chem. Soc. Rev.* **2009**, 38 (9), 2520–2531.
- (4) Tarascon, J.-M.; Armand, M. Issues and Challenges Facing Rechargeable Lithium Batteries. *Nature* **2001**, *414*, 359.
- (5) Hu, Y.-Y.; Liu, Z.; Nam, K.-W.; Borkiewicz, O. J.; Cheng, J.; Hua, X.; Dunstan, M. T.; Yu, X.; Wiaderek, K. M.; Du, L.-S.; et al. Origin of Additional Capacities in Metal Oxide Lithium-Ion Battery Electrodes. *Nat. Mater.* **2013**, *12*, 1130.
- (6) Liu, D.-R.; Williams, D. B. The Electron-Energy-Loss Spectrum of Lithium Metal. *Philos. Mag. B* **1986**, *53* (6), L123–L128.
- (7) Cheng, X.-B.; Zhang, R.; Zhao, C.-Z.; Wei, F.; Zhang, J.-G.; Zhang, Q. A Review of Solid Electrolyte Interphases on Lithium Metal Anode. *Adv. Sci.* **2016**, *3* (3), 1500213.
- (8) Introduction To Focused Ion Beams; Giannuzzi, L. A., Stevie, F. A., Eds.; Springer: Boston, MA, 2005.
- (9) Krueger, R. Dual-Column (FIB-SEM) Wafer Applications. *Micron* 1999, 30 (3), 221-226.

- (10) Zhu, Y.; Espinosa, H. D. An Electromechanical Material Testing System for *in Situ* Electron Microscopy and Applications. *Proc. Natl. Acad. Sci. U. S. A.* **2005**, *102* (41), 14503–14508.
- (11) Iwai, H.; Shikazono, N.; Matsui, T.; Teshima, H.; Kishimoto, M.; Kishida, R.; Hayashi, D.; Matsuzaki, K.; Kanno, D.; Saito, M.; et al. Quantification of SOFC Anode Microstructure Based on Dual Beam FIB-SEM Technique. *J. Power Sources* **2010**, *195* (4), 955–961.
- (12) Dubochet, J.; Adrian, M.; Chang, J. J.; Homo, J. C.; Lepault, J.; McDowall, A. W.; Schultz, P. Cryo-Electron Microscopy of Vitrified Specimens. Q. Rev. Biophys. 1988, 21 (2), 129–228.
- (13) Zachman, M. J.; Asenath-Smith, E.; Estroff, L. A.; Kourkoutis, L. F. Site-Specific Preparation of Intact Solid–Liquid Interfaces by Label-Free In Situ Localization and Cryo-Focused Ion Beam Lift-Out. *Microsc. Microanal.* **2016**, 22 (6), 1338–1349.
- (14) Zachman, M. J.; Tu, Z.; Choudhury, S.; Archer, L. A.; Kourkoutis, L. F. Cryo-STEM Mapping of Solid-Liquid Interfaces and Dendrites in Lithium-Metal Batteries. *Nature* **2018**, *560* (7718), 345–349.
- (15) Dolph, M. C.; Santeufemio, C. Exploring Cryogenic Focused Ion Beam Milling as a Group III—V Device Fabrication Tool. *Nucl. Instrum. Methods Phys. Res., Sect. B* **2014**, 328, 33–41.
- (16) Desbois, G.; Urai, J. L.; Burkhardt, C.; Drury, M. R.; Hayles, M.; Humbel, B. Cryogenic Vitrification and 3D Serial Sectioning Using High Resolution Cryo-FIB SEM Technology for Brine-Filled Grain Boundaries in Halite: First Results. *Geofluids* **2008**, 8 (1), 60–72.
- (17) Sardashti, K.; Haight, R.; Anderson, R.; Contreras, M.; Fruhberger, B.; Kummel, A. C. Grazing Incidence Cross-Sectioning of Thin-Film Solar Cells via Cryogenic Focused Ion Beam: A Case Study on CIGSe. ACS Appl. Mater. Interfaces 2016, 8 (24), 14994—14999.
- (18) Bakhsh, T. A.; Sadr, A.; Mandurah, M. M.; Shimada, Y.; Zakaria, O.; Tagami, J. In Situ Characterization of Resin-Dentin Interfaces Using Conventional vs. Cryofocused Ion-Beam Milling. *Dent. Mater.* **2015**, *31* (7), 833–844.
- (19) Bakhsh, T. A. Ultrastructural Features of Dentinoenamel Junction Revealed by Focused Gallium Ion Beam Milling. *J. Microsc.* **2016**, 264 (1), 14–21.
- (20) Tu, Z.; Zachman, M. J.; Choudhury, S.; Khan, K. A.; Zhao, Q.; Kourkoutis, L. F.; Archer, L. A. Stabilizing Protic and Aprotic Liquid Electrolytes at High-Bandgap Oxide Interphases. *Chem. Mater.* **2018**, 30 (16), 5655–5662.
- (21) Lee, J. Z.; Wynn, T. A.; Schroeder, M. A.; Alvarado, J.; Wang, X.; Xu, K.; Meng, Y. S. Cryogenic Focused Ion Beam Characterization of Lithium Metal Anodes. *ACS Energy Lett.* **2019**, 4 (2), 489–493.
- (22) Ballerini, M.; Milani, M.; Batani, D.; Squadrini, F. Focused Ion Beam Techniques for the Analysis of Biological Samples: A Revolution in Ultramicroscopy? *Proc. SPIE* **2001**, *4261*, 92–104.
- (23) Heymann, J. a W.; Hayles, M.; Gestmann, I.; Giannuzzi, L. a.; Lich, B.; Subramaniam, S. Site-Specific 3D Imaging of Cells and Tissues with a Dual Beam Microscope. *J. Struct. Biol.* **2006**, *155* (1), 63–73.
- (24) Villa, E.; Schaffer, M.; Plitzko, J. M.; Baumeister, W. Opening Windows into the Cell: Focused-Ion-Beam Milling for Cryo-Electron Tomography. *Curr. Opin. Struct. Biol.* **2013**, *23*, 771–777.
- (25) Marko, M.; Hsieh, C.; Schalek, R.; Frank, J.; Mannella, C. Focused-Ion-Beam Thinning of Frozen-Hydrated Biological Specimens for Cryo-Electron Microscopy. *Nat. Methods* **2007**, *4*, 215.
- (26) Rigort, A.; Villa, E.; Bäuerlein, F. J. B.; Engel, B. D.; Plitzko, J. M. Integrative Approaches for Cellular Cryo-Electron Tomography: Correlative Imaging and Focused Ion Beam Micromachining; Elsevier, 2012; Vol. 111.
- (27) Arnold, J.; Mahamid, J.; Lucic, V.; De Marco, A.; Fernandez, J. J.; Laugks, T.; Mayer, T.; Hyman, A. A.; Baumeister, W.; Plitzko, J. M. Site-Specific Cryo-Focused Ion Beam Sample Preparation Guided by 3D Correlative Microscopy. *Biophys. J.* **2016**, *110* (4), 860–869.
- (28) Harapin, J.; Börmel, M.; Sapra, K. T.; Brunner, D.; Kaech, A.; Medalia, O. Structural Analysis of Multicellular Organisms with Cryo-Electron Tomography. *Nat. Methods* **2015**, *12* (7), 634–636.

- (29) Noble, J. M.; Lubieniecki, J.; Savitzky, B. H.; Plitzko, J.; Engelhardt, H.; Baumeister, W.; Kourkoutis, L. F. Connectivity of Centermost Chromatophores in Rhodobacter Sphaeroides Bacteria. *Mol. Microbiol.* **2018**, *109* (6), 812–825.
- (30) Rubino, S.; Akhtar, S.; Melin, P.; Searle, A.; Spellward, P.; Leifer, K. A site-specific focused-ion-beam lift-out method for cryo Transmission Electron Microscopy. *J. Struct. Biol.* **2012**, *180*, 572–576.
- (31) Mahamid, J.; Schampers, R.; Persoon, H.; Hyman, A. A.; Baumeister, W.; Plitzko, J. M. A Focused Ion Beam Milling and Lift-out Approach for Site-Specific Preparation of Frozen-Hydrated Lamellas from Multicellular Organisms. *J. Struct. Biol.* **2015**, *192* (2), 262–269.
- (32) Li, Y.; Li, Y.; Sun, Y.; Butz, B.; Yan, K.; Koh, A. L.; Zhao, J.; Pei, A.; Cui, Y. Revealing Nanoscale Passivation and Corrosion Mechanisms of Reactive Battery Materials in Gas Environments. *Nano Lett.* **2017**, *17* (8), 5171–5178.
- (33) Li, Y.; Li, Y.; Pei, A.; Yan, K.; Sun, Y.; Wu, C. L.; Joubert, L. M.; Chin, R.; Koh, A. L.; Yu, Y.; et al. Atomic Structure of Sensitive Battery Materials and Interfaces Revealed by Cryo-Electron Microscopy. *Science* **2017**, 358, 506–510.
- (34) Wang, X.; Zhang, M.; Alvarado, J.; Wang, S.; Sina, M.; Lu, B.; Bouwer, J.; Xu, W.; Xiao, J.; Zhang, J.-G.; et al. New Insights on the Structure of Electrochemically Deposited Lithium Metal and Its Solid Electrolyte Interphases via Cryogenic TEM. *Nano Lett.* **2017**, *17* (12), 7606–7612.
- (35) Sangster, J.; Pelton, A. D. The Ga-Li (Gallium-Lithium) System. J. Phase Equilib. 1991, 12 (1), 33–36.
- (36) Okamoto, H. Ga-Li (Gallium-Lithium). *J. Phase Equilib. Diffus.* **2006**, 27 (2), 200.
- (37) Rosenblatt, S.; Yaish, Y.; Park, J.; Gore, J.; Sazonova, V.; McEuen, P. L. High Performance Electrolyte Gated Carbon Nanotube Transistors. *Nano Lett.* **2002**, 2 (8), 869–872.
- (38) Prasad, B.; Pfanzelt, G.; Fillis-Tsirakis, E.; Zachman, M. J.; Kourkoutis, L. F.; Mannhart, J. Integrated Circuits Comprising Patterned Functional Liquids. *Adv. Mater.* **2018**, *30* (35), 1802598.
- (39) Schlom, D. G. Perspective: Oxide Molecular-Beam Epitaxy Rocks! *APL Mater.* **2015**, 3 (6), 062403.
- (40) Tu, Z.; Choudhury, S.; Zachman, M. J.; Wei, S.; Zhang, K.; Kourkoutis, L. F.; Archer, L. A. Designing Artificial Solid-Electrolyte Interphases for Single-Ion and High-Efficiency Transport in Batteries. *Joule* **2017**, *1* (2), 394–406.
- (41) Tu, Z.; Choudhury, S.; Zachman, M. J.; Wei, S.; Zhang, K.; Kourkoutis, L. F.; Archer, L. A. Fast Ion Transport at Solid–Solid Interfaces in Hybrid Battery Anodes. *Nat. Energy* **2018**, 3 (4), 310–316.
- (42) Choudhury, S.; Wei, S.; Ozhabes, Y.; Gunceler, D.; Zachman, M. J.; Tu, Z.; Shin, J. H.; Nath, P.; Agrawal, A.; Kourkoutis, L. F.; et al. Designing Solid-Liquid Interphases for Sodium Batteries. *Nat. Commun.* **2017**, *8* (1), 898.
- (43) Choudhury, S.; Wan, C. T.-C.; Al Sadat, W. I.; Tu, Z.; Lau, S.; Zachman, M. J.; Kourkoutis, L. F.; Archer, L. A. Designer Interphases for the Lithium-Oxygen Electrochemical Cell. *Sci. Adv.* **2017**, *3* (4), No. e1602809.
- (44) Kang, S.-H.; Goodenough, J. B.; Rabenberg, L. K. Nanocrystalline Lithium Manganese Oxide Spinel Cathode for Rechargeable Lithium Batteries. *Electrochem. Solid-State Lett.* **2001**, *4* (5), A49—A51.
- (45) Xu, K. Nonaqueous Liquid Electrolytes for Lithium-Based Rechargeable Batteries. *Chem. Rev.* **2004**, *104* (10), 4303–4417.
- (46) Manthiram, A.; Chemelewski, K.; Lee, E.-S. A Perspective on the High-Voltage LiMn1.5Ni0.5O4 Spinel Cathode for Lithium-Ion Batteries. *Energy Environ. Sci.* **2014**, 7 (4), 1339–1350.
- (47) Levin, B. D. A.; Zachman, M. J.; Werner, J. G.; Sahore, R.; Nguyen, K. X.; Han, Y.; Xie, B.; Ma, L.; Archer, L. A.; Giannelis, E. P.; et al. Characterization of Sulfur and Nanostructured Sulfur Battery Cathodes in Electron Microscopy without Sublimation Artifacts. *Microsc. Microanal.* 2017, 23 (1), 155–162.

- (48) Bruce, P. G.; Freunberger, S. A.; Hardwick, L. J.; Tarascon, J.-M. Li-O<sub>2</sub> and Li-S Batteries with High Energy Storage. *Nat. Mater.* **2012**, *11* (December 2011), 19–29.
- (49) Burnett, T. L.; Kelley, R.; Winiarski, B.; Contreras, L.; Daly, M.; Gholinia, A.; Burke, M. G.; Withers, P. J. Large Volume Serial Section Tomography by Xe Plasma FIB Dual Beam Microscopy. *Ultramicroscopy* **2016**, *161*, 119–129.
- (50) Xiaobing, L.; Holland, J.; Burgess, S.; Bhadare, S.; Yamaguchi, S.; Birtwistle, D.; Statham, P.; Rowlands, N. Detection of Lithium X-Rays by EDS. *Microsc. Microanal.* **2013**, *19* (Suppl 2), 1136–1137.
- (51) Echlin, P. Low-Temperature Microscopy and Analysis; Springer Science+Business Media: New York, 1992.
- (52) Warkentin, M.; Sethna, J. P.; Thorne, R. E. Critical Droplet Theory Explains the Glass Formability of Aqueous Solutions. *Phys. Rev. Lett.* **2013**, *110* (1), 015703.
- (53) Tivol, W. F.; Briegel, A.; Jensen, G. J. An Improved Cryogen for Plunge Freezing. *Microsc. Microanal.* **2008**, *14* (5), 375–379.
- (54) Kesselman, E.; Talmon, Y.; Bang, J.; Abbas, S.; Li, Z.; Lodge, T. P. Cryogenic Transmission Electron Microscopy Imaging of Vesicles Formed by a Polystyrene-Polyisoprene Diblock Copolymer. *Macromolecules* **2005**, 38 (16), 6779–6781.
- (55) Koifman, N.; Schnabel-Lubovsky, M.; Talmon, Y. Nanostructure Formation in the Lecithin/Isooctane/Water System. *J. Phys. Chem. B* **2013**, 117 (32), 9558–9567.
- (56) Oostergetel, G. T.; Esselink, F. J.; Hadziioannou, G. Cryo-Electron Microscopy of Block Copolymers in an Organic Solvent. *Langmuir* 1995, 11 (10), 3721–3724.
- (57) Boettcher, C.; Schade, B.; Fuhrhop, J. H. Comparative Cryo-Electron Microscopy of Noncovalent N-Dodecanoyl-(D- and L-) Serine Assemblies in Vitreous Toluene and Water. *Langmuir* **2001**, *17* (3), 873–877.
- (58) Danino, D.; Gupta, R.; Satyavolu, J.; Talmon, Y. Direct Cryogenic-Temperature Transmission Electron Microscopy Imaging of Phospholipid Aggregates in Soybean Oil. *J. Colloid Interface Sci.* **2002**, 249 (1), 180–186.
- (59) Hayles, M. F.; Stokes, D. J.; Phifer, D.; Findlay, K. C. A Technique for Improved Focused Ion Beam Milling of Cryo-Prepared Life Science Specimens. *J. Microsc.* **2007**, 226 (Pt 3), 263–269.